water

MDPI

Article

Variability of δ^2H and $\delta^{18}O$ in Soil Water and Its Linkage to Precipitation in an East Asian Monsoon Subtropical Forest Plantation

Sidan Lyu

Key Laboratory of Ecosystem Network Observation and Modeling, Institute of Geographic Sciences and Natural Resources Research, Chinese Academy of Sciences, Beijing 100101, China; lvsidan@igsnrr.ac.cn

Abstract: The linkage between δ^2H and $\delta^{18}O$ of soil water and precipitation provides a way of understanding precipitation infiltration, residence time, and soil water source. Soil water at 0–5, 15–20, and 40–45 cm depths and event-based precipitation were collected in a subtropical forest plantation. Correlations between the $\delta^{18}O$ of soil water and precipitation on the same day were used to determine the critical threshold of precipitation infiltration. Residence time of precipitation in soil was determined with correlations between the $\delta^{18}O$ of soil water and cumulative precipitation before sampling. Soil water source was determined by the intersection points of Soil Water Evaporation Lines (SEL) and local meteoric water lines. The results showed that precipitation >5–6 mm could pass through canopy and litter, and infiltrate into soil. Residence times varied from a few days to several months, and increased with soil depth. The model-based approach for SEL estimation were more robust than the regression-based approach due to the inverse variability in the δ^2H and $\delta^{18}O$ of soil water source and soil evaporative fractionation. Soil water at a 0–5 cm depth originated mainly from precipitation in the current season, while those at 15–20 and 40–45 cm depths originated mainly from precipitation in the previous season.

Keywords: stable isotopes; soil water; precipitation infiltration; residence time; soil water source; seasonal variation; East Asian monsoon region

Citation: Lyu, S. Variability of δ^2H and $\delta^{18}O$ in Soil Water and Its Linkage to Precipitation in an East Asian Monsoon Subtropical Forest Plantation. *Water* **2021**, *13*, 2930. https://doi.org/10.3390/w13202930

Academic Editors: Polona Vreča and Zoltán Kern

Received: 2 September 2021
Accepted: 15 October 2021
Published: 19 October 2021

1. Introduction

Soil water, as a key link in the hydrological cycle, partitions precipitation into evaporation, transpiration, and runoff [1]. Precipitation is the main source of soil water replenishment, and it controls the mixing and redistribution of soil water [2]. The linkage of soil water with precipitation is increasingly relevant due to the changes in rain patterns caused by climate change [3]. δ^2H and $\delta^{18}O$ in water have been widely used as ideal tracers of water movement and mixing among different water pools [4]. δ^2H and $\delta^{18}O$ in soil water can largely retain the isotopic signal of precipitation due to the infiltration of precipitation larger than a certain amount, and by the lack of fractionation during root water uptake, except that by some halophytes or woody xerophytes [5,6]. Nevertheless, soil evaporation can result in the enrichment of soil water in heavy isotopes [7]. The linkage between δ^2H and $\delta^{18}O$ in soil water and precipitation is useful for the understanding of precipitation infiltration, residence time, and soil water source [8].

The replenishment of soil water occurs only via precipitation that exceeds the critical threshold—the amount that is lost to canopy interception or litter retention [9]. The determination of the critical threshold for the precipitation recharge of soil water is central to the accurate estimation of soil water replenishment and water balance [2,9]. Some authors have estimated this threshold with throughfall measurements using rain-gauges and determined that it corresponded to throughfall when precipitation was 0 based on linear regression between the two [10]. Others used the relationship between the variability in soil water content and precipitation amount to estimate this threshold [11]. However,

δ^2H and $\delta^{18}O$ in precipitation directly influences those in soil water due to precipitation infiltration, and their linkage can be used for analyzing soil water replenishment such as the ecohydrological separation [12] or connectivity [13] between soil-bound and mobile water.

Knowledge of the residence time of precipitation in the soil profile helps to better understand hydrological processes and timescales of transport, and to improve hydrological models [14]. Tracers and hydrological models are usually used for estimating residence times of precipitation in soil [15]. Natural variation in δ^2H and $\delta^{18}O$ in soil water can be used to date water for up to 5 years, depending on the mixing and dispersion across the soil profile [4]. Hydrological models (e.g., HYDRUS-1D, which can simulate the one-dimensional movement of water and multiple solutes in variably saturated porous media) can also be used to simulate residence times by tracking the travel time of water particles as they flow through a soil profile [16]. Although these models may allow researchers to link residence times with specific hydrological processes, they are based on the assumption that soil water is well mixed in pore space, which is in contrast to recent evidence that soil water can be distinguished into soil-bound and mobile water [1]. Existing studies showed that residence times of precipitation in soils typically span from hours to years due to the integrated influences of precipitation input, connectivity of soil pores, plants water uptake, and so on [15].

Soil water may be recharged by precipitation from the past rather than recent seasons due to the interactions between the mixtures of two soil water pools and variations in flow pathways, and the understanding of the seasonal origins of soil water remains limited [17]. Soil Water Evaporation Lines (SEL, the trend line of δ^2H and $\delta^{18}O$ in soil water in dual-isotope space) deviated from Local Meteoric Water Lines (LMWL, a regression line between δ^2H and $\delta^{18}O$ values in precipitation) due to fractionation effects of soil evaporation [17,18]. To compensate for these fractionation effects, the intersection points of SEL and LMWL can be interpreted as the δ^2H and $\delta^{18}O$ in the soil water source [18,19]. SEL has been estimated by using theoretical model-based approaches and regression-based approaches with data from soil water samples [20]. Some authors reported that when isotopic variability in precipitation or the seasonal variability in evaporation fractionation of soil water were large, the SEL calculated with theoretical model-based approaches was more robust than that calculated with the regression-based approaches [21]. Using the Craig and Gordon model for the theoretical modeling of evaporative isotopic fractionation for diffusion-controlled soil evaporation scenarios in estimating SEL, Xiang et al. [22] found that deep soil water in the Loess Plateau of China originated mainly from rainy season precipitation.

In this study, we analyzed δ^2H and $\delta^{18}O$ in soil water extracted from soil samples at 0–5, 15–20, and 40–45 cm depths, and event-based precipitation in an East Asian monsoon subtropical forest plantation. The critical threshold for the precipitation recharge of soil water was determined with correlations between δ^2H and $\delta^{18}O$ in soil water and precipitation on the same day. The residence time of precipitation in soil was determined with correlations between δ^2H and $\delta^{18}O$ in soil water and cumulative precipitation before soil sampling. Soil water source was determined by using the intersection points of LMWL and SEL calculated with regression-based and Craig and Gordon model-based approaches. The objectives of our study were: (1) to investigate how much precipitation could pass through the canopy and litter, and infiltrate into the soil; (2) to determine seasonal variability in the residence times of precipitation at different soil depths; (3) to compare the regression-based and Craig and Gordon model-based approaches for estimating SEL, and analyze the seasonal origins of soil water.

2. Materials and Methods

2.1. Study Site

This study was conducted at Qianyanzhou (QYZ) Ecological Experimental Station (26°44′52″ N, 115°39′47″ E, and elevation 102 m) of the Chinese Ecosystem Research Network (CERN), a member of ChinaFLUX, located in Taihe County, Jiangxi Province in southern China (Figure 1). The climate in the area is controlled by the Western Pacific

subtropical high and subtropical East Asian monsoon [23]. Annual precipitation and mean air temperature for the period of 1985–2020 were 1407.3 ± 300.2 mm and 18.1 ± 0.5 °C, respectively, according to the meteorological records of CERN (Table 1). The whole year was divided into winter (December–February), spring (March–May), summer (June–August), and autumn (September–November) according to air temperatures [24,25]. More than half of the annual precipitation (68%) takes place in spring (32%) and summer (36%), while the mean air temperature peaked in summer (Table 1).

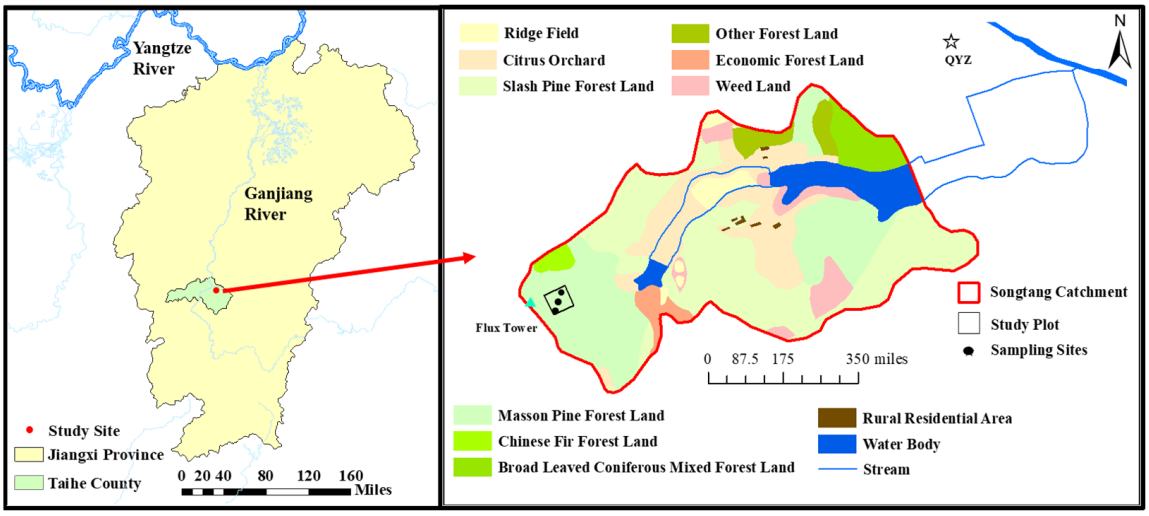

Figure 1. Map of study site location and soil sampling location.

Table 1. Climate, soil, and vegetation characteristics of the study site.

Climate	Month	P (mm)	T_a (°C)	RH (%)	P_a (hPa)	WS (m/s)
	1	72.0	6.4	86.8	1013.1	2.5
	2	98.1	8.8	87.0	1010.3	3.0
	3	150.9	12.3	86.3	1007.4	2.9
	4	162.3	18.5	85.1	1003.1	3.0
	5	177.5	23.0	84.2	999.2	2.8
	6	217.0	26.3	84.0	995.5	2.7
	7	117.9	28.7	77.4	994.9	3.4
	8	138.9	28.0	81.5	995.6	2.6
	9	88.0	24.6	83.9	1000.7	2.5
	10	60.5	19.3	82.7	1006.8	2.4
	11	73.2	13.5	81.7	1010.0	2.4
	12	51.0	7.8	83.8	1013.2	2.3
Soil	**pH**	**BD (g/cm^3)**	**Sand (%)**	**Silt (%)**	**Clay (%)**	**T_s (°C)**
	4.04–6.25	1.57	17	68	15	7.2–26.0
Vegetation	**TD (stems/ha)**	**TB (t/ha)**	**LAI_{max} (m^2/m^2)**			
	1463	106	5.6			

P is precipitation; T_a is air temperature; RH is relative humidity; P_a is atmospheric pressure; WS is wind speed; BD is soil bulk density; T_s is soil temperature; TD is tree density; TB is total biomass; LAI_{max} is maximum of leaf area index.

The study plot (100 × 100 m^2) was at the top of a hill located within the Songtang catchment of QYZ (Figure 1), where soil depth is less than 100 cm, and average groundwater level is about 3.43 m. The soil at the site is red earth weathered from sandstone, sandy conglomerate, mudstone, and alluvium. Soil bulk density, sand, silt, and clay contents, and soil temperature are shown in Table 1 [26]. The subtropical forest plantation at the site was planted around 1985, and the dominant tree species were Masson pine (*Pinus massoniana* L.), slash pine (*Pinus elliottii* E.), and Chinese fir (*Cunninghamia lanceolata* L.) [27].

The growing season lasts from March to October. The tree density, the total biomass, and the maximum of leaf area index are shown in Table 1 [28].

The QYZ station (http://qya.cern.ac.cn, accessed on 26 August 2021) operates an above-canopy flux system for ecosystem evapotranspiration and CO_2 flux measurements. The flux system was mounted on a tower at 39.6 m, and consisted of an open-path CO_2/H_2O analyzer (LI-7500, Licor Inc., Lincoln, NE, USA) and a three-dimensional sonic anemometer (CSAT3, Campbell Scientific Inc., Logan, UT, USA). Flux variables were sampled at 10 Hz using a CR5000 datalogger (Model CR5000, Campbell Scientific Inc., Logan, UT, USA), and 30 min mean fluxes were calculated [28]. Air temperature and relative humidity were measured with a temperature and humidity sensor (HMP45C, Vaisala Inc., Helsinki, Finland). Precipitation was monitored with a rain gauge (RG13H, Vaisala Inc., Helsinki, Finland). A pressure sensor (DPA501, Delta Electronics Inc., Taibei, China) was used for measuring atmospheric pressure. Wind speed was monitored with an anemoscope (WAA151, Vaisala Inc., Helsinki, Finland). These meteorological variables were collected every 1 h.

2.2. Sample Collection and Measurements

Soil samples were collected 2–3 times per week from January 2012 to March 2015, and 2 times per month (early and last days of each month) from April 2015 to December 2017, for δ^2H and $\delta^{18}O$ isotopic analyses. Soil samples at 0–5, 15–20, and 40–45 cm depths were collected with a hollow-stem auger (0.04 m in diameter and 0.25 m in length), and three replicate soil samples at each depth range were randomly taken in the sampling plot. All soil samples were stored in a refrigerator at −15 °C up to −20 °C until soil water extraction.

Precipitation was collected in a polyethylene bottle fitted with a funnel and topped with a ping-pong ball to prevent evaporation [26]. The end of a precipitation event was identified as the point after 6 h of no precipitation from the moment this precipitation had stopped. Precipitation samples were collected after each precipitation event from January 2011 to December 2017. All precipitation samples were refrigerated at 4 °C before isotope analysis.

In total, 3514 soil samples and 520 precipitation samples were collected during the study period. A week after sampling, soil water was extracted from soil samples with a cryogenic vacuum distillation system, with heating at >90 °C and an extraction time of 0.5–1.5 h, depending on soil water content [29]. In order to determine soil water extraction efficiency, pre- and post-water extraction soil sample weights as well as sample weights after additional oven-drying (105 °C, 48 h) were compared [29]. In this study, the extraction efficiency of water from soil samples was higher than 98.0%. Soil water and precipitation were filtered through a 0.45 µm mixed cellulose membrane (Jiuding Gaoke Co. Ltd., Beijing, China), and 2 mL of water samples was used for the analysis of δ^2H and $\delta^{18}O$.

δ^2H and $\delta^{18}O$ were analyzed using an Isotopic Ratio Infrared Spectroscopy (IRIS) system (Model DLT-100; Los Gatos Research Inc., San Jose, CA, USA) [30]. The number of injections into IRIS were 6, and the results of the last three injections were used for analysis. The results were normalized to Vienna Standard Mean Ocean Water (VSMOW), and expressed in the standard δ notation (in‰):

$$\delta_{sample}(\frac{0}{00}) = \left(\frac{R_{sample}}{R_{VSMOW}} - 1\right) \times 1000 \quad (1)$$

where δ_{sample} is the δ^2H and $\delta^{18}O$ of the sample, and R_{sample} and R_{VSMOW} are the ratio of $^{18}O/^{16}O$ or $^{2}H/^{1}H$ in the sample and in the *VSMOW*, respectively. For the quality control of IRIS, commercial reference materials LGR3E, LGR5E, and LGR4 (Los Gatos Research Inc., San Jose, CA, USA) were used. The measurement precision of the liquid water isotope analyzer was 0.3‰ for δ^2H, and 0.1‰ for $\delta^{18}O$. Soil Water Content (SWC) was calculated as SWC (cm^3/cm^3) = ((fresh weight − dry weight)/(dry weight)) × soil bulk density.

2.3. Data Analysis

2.3.1. Critical Thresholds for Precipitation Recharge of Soil Water

Same-day soil water and precipitation samples (n = 94) were selected in order to determine the critical thresholds for the precipitation recharge of soil water—when precipitation larger than this threshold can pass through the canopy and litter, and infiltrate into the soil. Correlation coefficients between δ^2H and δ^{18}O in selected soil water at each depth (0–5, 15–20, and 40–45 cm) and precipitation were calculated. Precipitation was classified into different precipitation amounts, including ≥0.2, 0.4, 0.6, 0.8, 1, 1.2, 1.6, 2, 2.4, 2.8, 4, 5, 6, 8, 11, and 15.5 mm. The threshold was determined to be the precipitation amount when correlation coefficients between δ^2H and δ^{18}O in soil water and precipitation that is larger than the precipitation amount were more than the coefficients between δ^2H and δ^{18}O in soil water and precipitation less than the precipitation amount, based on the graphical inference or statistical methods.

There were no significant differences ($p > 0.05$) among the triplicates of soil water samples according to multiple comparisons. Weighted mean δ^2H and δ^{18}O for soil water ($\delta_{s,mean}$) was obtained by weighting the soil water content of each sample, and using the following equations:

$$\delta_{s,mean} = \sum_{i=1}^{3}(\theta_i \times \delta_{s,i}) / \sum_{i=1}^{3}\theta_i \quad (2)$$

where θ_i is the soil water content of the ith soil sample replicate; $\delta_{s,i}$ is the δ^2H and δ^{18}O of the ith soil sample replicate; i is the number of the soil sample replicate.

2.3.2. Determining Residence Times of Precipitation in Soil

Correlation coefficients between δ^2H and δ^{18}O in soil water and the cumulative precipitation before soil sampling were calculated. Only precipitation larger than the critical thresholds for the precipitation recharge of soil water were analyzed. Cumulative precipitation was calculated for periods of 0, 2, 7, 15, 30, 45, 60, 75, 90, 105, 120, 135, and 150 days before sampling due to the collection frequency of soil at an average of 2 or 8–12 times per month. The residence time of precipitation after entering the soil profile was determined as that period of time (from 0 to 150 days) when correlation coefficients were the highest. Residence times at 0–5, 15–20, and 40–45 cm depths during winter, spring, summer, and autumn, respectively, were calculated.

The weighted means of δ^2H and δ^{18}O for precipitation ($\delta_{p,mean}$) were obtained by weighting the amount of precipitation for each precipitation event, and calculated as:

$$\delta_{p,mean} = \left(\sum_{i=1}^{n}\delta_{p,i} \times PPT_i\right) / \left(\sum_{i=1}^{n} PPT_i\right) \quad (3)$$

where $\delta_{p,i}$ is the δ^2H and δ^{18}O of the ith precipitation event, PPT_i is the amount of the ith precipitation event. The precipitation samples that significantly deviated from the LMWL were eventually excluded. Machine learning [31] was used for predicting the missing δ^2H and δ^{18}O of the precipitation event after data quality control. We used random forests to train data and learn relationships between predictors and outcomes. Precipitation, air temperature, vapor concentration, atmospheric pressure, relative humidity, atmospheric vapor pressure deficit (VPD), wind speed, evapotranspiration (ET), and outgoing longwave radiation value (OLR, downloaded from NOAA Climate Data Record) were selected as predictors for the training of machine learning models. The calendar seasons were added as fuzzy sets in the model. A total of 80% of the precipitation event samples was randomly selected as the training subset, and the remaining 20% of the samples was selected as the validation subset. The Root Mean Squared Errors (RMSE) of prediction using random forests were 16.90 for δ^2H, and 2.04 for δ^{18}O, respectively. There was no significant difference between the magnitude of results obtained by predicting the missing data and only the measured data.

2.3.3. Calculations of δ^2H and $\delta^{18}O$ in Soil Water Source

(1) Calculations of Soil Water Evaporation Line

In order to determine if the regression-based approach was valid, SEL was calculated by the regression-based and Craig and Gordon model-based approaches. The regression-based approach is defined as a linear regression between the δ^2H and $\delta^{18}O$ values in soil water taken from a depth profile [32]:

$$\delta^2H = a_{SEL} \times \delta^{18}O + b_{SEL} \quad (4)$$

where a_{SEL} and b_{SEL} represent the slope and intercept of SEL.

For the Craig and Gordon model-based approach, the slope of SEL (S_{SEL}) in a soil water pool fed by local precipitation is predicted by the Craig and Gordon model [33]:

$$S_{SEL} = \frac{\left[\frac{h(\delta_A-\delta_P)+(1+\delta_P)(\varepsilon_K+\varepsilon^+/\alpha^+)}{h-\varepsilon_K-\varepsilon^+/\alpha^+}\right]_2}{\left[\frac{h(\delta_A-\delta_P)+(1+\delta_P)(\varepsilon_K+\varepsilon^+/\alpha^+)}{h-\varepsilon_K-\varepsilon^+/\alpha^+}\right]_{18}} \quad (5)$$

where h is the relative humidity, set to the mean relative humidity during the residence time; δ_P is the δ^2H and $\delta^{18}O$ in precipitation, set to the weighted average of δ^2H and $\delta^{18}O$ in precipitation during the residence time; δ_A is the δ^2H and $\delta^{18}O$ in ambient atmospheric vapor, and is determined using the precipitation-equilibrium assumption:

$$\delta_A = \left(\delta_P - \varepsilon^+\right)/\alpha^+ \quad (6)$$

α^+ is the liquid-vapor equilibrium isotopic fractionation, estimated from empirical relationships by Horita and Wesolowski [34]:

$$\text{for } \delta^{18}O,\ \ln\alpha^+ = \frac{0.35041}{(T_s+273.15)^3} \times 10^6 - \frac{1.6664}{(T_s+273.15)^2} \times 10^3 - \frac{6.7123}{(T_s+273.15)} - 7.685 \times 10^{-3} \quad (7)$$

$$\text{for } \delta^2H,\ \ln\alpha^+ = \frac{\text{for } \delta^2H,\ 2.9992}{(T_s+273.15)^3} \times 10^6 + 161.04 \times 10^{-3} + \frac{794.84}{10^6} \times (T_s+273.15) - \frac{1620.1}{10^9} \times (T_s+273.15)^2 + \frac{1158.8}{10^{12}} \times (T_s+273.15)^3 \quad (8)$$

where T_s is soil temperature at the evaporation front, set to the mean air temperature during the residence time.

ε^+ is the equilibrium isotopic separation between liquid and vapor, calculated as $\varepsilon^+(‰) = (\alpha^+ - 1) \times 10^3$. ε_K is the equivalent kinetic isotopic separation based on wind tunnel experiments [35], calculated as:

$$\varepsilon_k = n \times C_K^0 \times \theta \times (1-h) \quad (9)$$

where C_K^0 is 25.0 and 28.6% for deuterium and oxygen-18, respectively; n = 1 for soil water; $\theta = (1-h')/(1-h)$ is an advection term to account for the potential influence of humidity, often set to $\theta \approx 1$ for small water bodies, and h' is the adjusted humidity of the downwind atmosphere following the admixture of evaporating moisture over the surface.

Intercept of SEL (I_{SEL}) is calculated with δ^2H and $\delta^{18}O$ in soil water (δ^2H_s and $\delta^{18}O_s$) as follows:

$$I_{SEL} = \delta^2H_s - S_{SEL} \times \delta^{18}O_s \quad (10)$$

(2) δ^2H and $\delta^{18}O$ in Soil Water Source

δ^2H and $\delta^{18}O$ in soil water source were calculated using the intersection points of SEL with LMWL [19]:

$$\delta^{18}O_{\text{intersect}} = \frac{b_{SEL}-b}{a-a_{SEL}} \quad (11)$$

$$\delta D_{\text{intersect}} = a\delta^{18}O_{\text{intersect}} + b \quad (12)$$

where a_{SEL} and b_{SEL} represent the slope and intercept of SEL, and a and b represent the slope and intercept of LMWL.

δ^2H and $\delta^{18}O$ in precipitation >5 mm were used for fitting LMWL according to the following analysis of the critical thresholds for the precipitation recharge of soil water. The slopes or intercepts of LMWL in spring, summer, autumn, and winter were calculated using an ordinary least squares regression (OLSR). However, the precipitation amount weighted reduced major axis regression (PWRMA) may be more suitable for calculating LMWL, according to [36]. OLSR, reduced major axis regression (RMA), major axis regression (MA), and the corresponding precipitation weighted regressions (PWLSR, PWRMA, and PWMA) were compared by analyzing the calculated slopes and intercepts of LMWL, the average Root Mean Sum of Squared Error value of the fit ($RMSE_{av}$), and the significance in the difference of each regression to that of OLSR, according to [36] (Table S1). Although the slopes produced by OLSR were slightly less than those determined by PWRMA with the lowest $RMSE_{av}$, there was no significant difference between those produced by OLSR and PWRMA ($p > 0.05$).

2.3.4. Statistical Analyses

Linear regression was used for analyzing correlations between δ^2H and $\delta^{18}O$ in soil water and precipitation with the SPSS 22.0 software. For the comparison of δ^2H and $\delta^{18}O$ in soil water or soil water source at different soil depths with δ^2H and $\delta^{18}O$ in precipitation, a multiple comparison Tukey's post hoc test was used with the SPSS 22.0 software. $p < 0.05$ was considered statistically significant at a 95% confidence interval. Pearson correlation coefficients were calculated using the R studio 3.5.0.

3. Results

3.1. Seasonal Variability of δ^2H and $\delta^{18}O$ in Soil Water and Precipitation

$\delta^{18}O$ is solely used for identifying the seasonal variability of δ^2H and $\delta^{18}O$ in soil water and precipitation in Sections 3.1–3.3, due to the very high consistency of the temporal variability of δ^2H and $\delta^{18}O$. Seasonal variability of $\delta^{18}O$ in precipitation exhibited firstly a depletion trend, and then an enrichment trend, with −4.05‰, −8.15‰, −7.40‰, and −6.34‰ in spring, summer, autumn, and winter, respectively (Table S2). In addition, with an increase in the amount of precipitation, the weighted mean $\delta^{18}O$ in precipitation gradually declined from −5.23‰, −5.05‰, −5.68‰, −6.50‰, −6.06‰ to −7.55‰ when the amount of precipitation was 0–5, 5–10, 10–20, 20–30, 30–40, and >40 mm/day, respectively (Table S2). The weighted mean $\delta^{18}O$ in precipitation for large rainfall events (>40 mm/day) was significantly more depleted than that of small rainfall events (<10 mm/day).

Seasonal variability of the weighted average $\delta^{18}O$ in soil water at a depth of 0–5 cm, with −4.37‰, −7.94‰, −6.61‰, and −6.00‰ during spring, summer, autumn, and winter, respectively, was similar to that in precipitation (Figure 2 and Table S2). The weighted average $\delta^{18}O$ in soil water at a depth of 15–20 cm was most enriched in spring at −4.62‰, followed by −7.83‰, −8.13‰, and −8.38‰ in winter, summer, and autumn, respectively. They were similar to $\delta^{18}O$ in precipitation during spring and summer, and more depleted than $\delta^{18}O$ in precipitation during autumn and winter (Figure 3). At a depth of 40–45 cm, the weighted average $\delta^{18}O$ in soil water was most enriched in spring at −5.40‰, followed by −7.20‰, −8.02‰, and −8.15‰ in summer, winter, and autumn, respectively. They were more enriched during summer, and more depleted during spring, autumn, and winter as compared with $\delta^{18}O$ in precipitation (Figure 3). However, in autumn and winter, the weighted average $\delta^{18}O$ in soil water at a depth of 0–5 cm was significantly more enriched than that at 15–20 and 40–45 cm depths (Table S2). In spring, the weighted average $\delta^{18}O$ in soil water at 0–5 and 15–20 cm depths were significantly more enriched than that at the 40–45 cm depth. Nevertheless, the weighted average $\delta^{18}O$ in soil water at depths of 0–5 and 15–20 cm in summer was significantly more depleted than that at the 40–45 cm depth.

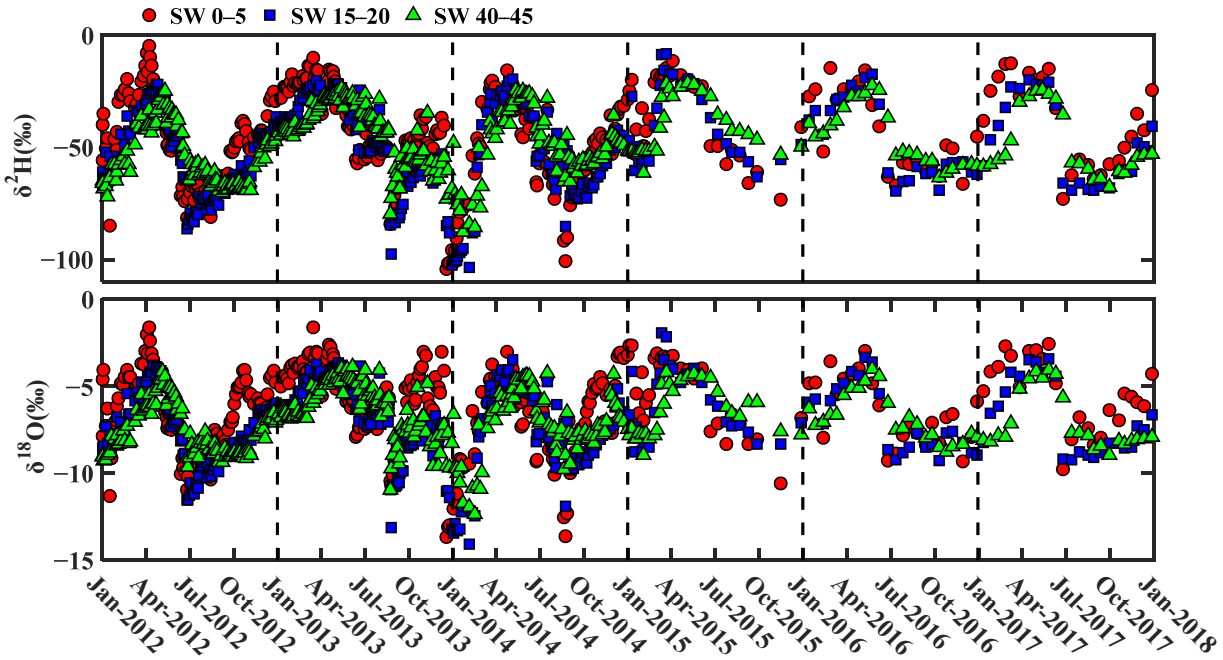

Figure 2. Temporal variability of δ^2H and $\delta^{18}O$ in soil water at depths of 0–5 (SW 0–5), 15–20 (SW 15–20), and 40–45 (SW 40–45) cm.

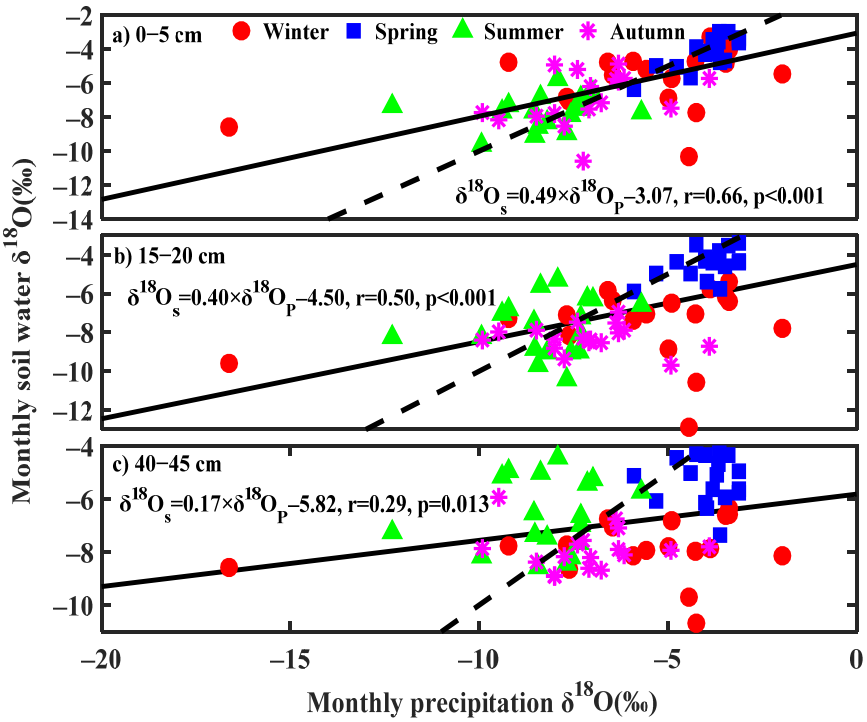

Figure 3. Relationships between monthly precipitation (weighted means by amount of precipitation, $\delta^{18}O_P$) and soil water (weighted means by soil water content, $\delta^{18}O_S$) for $\delta^{18}O$ at depths of (**a**) 0–5 cm, (**b**) 15–20 cm, and (**c**) 40–45 cm. Solid lines show regression lines between $\delta^{18}O_P$ and $\delta^{18}O_S$, and dashed lines show the 1:1 lines.

3.2. Critical Thresholds of Precipitation for Infiltration into the Soil Profile

Correlation coefficients between $\delta^{18}O$ in same-day soil water and precipitation larger than 6 mm were higher than those between $\delta^{18}O$ in same-day soil water and precipitation less than 6 mm, at 0–5, 15–20, and 40–45 cm soil depths (Figure 4). This indicates that precipitation larger than 6 mm passed through the canopy and litter layer, infiltrated into the soil, and significantly changed $\delta^{18}O$ in soil water. A critical threshold of precipitation for infiltration into the soil profile was determined to be 5–6 mm, and there were insufficient data to calculate correlation coefficients between $\delta^{18}O$ in same-day soil water and precipitation within the precipitation amount interval of 5–6 mm. Correlation coefficients between $\delta^{18}O$ in same-day soil water and precipitation increased with an increase in precipitation amount, and reached their largest values when precipitation amounts were $\geq$11 mm. The peak values of correlation coefficients decreased with an increase in soil depth.

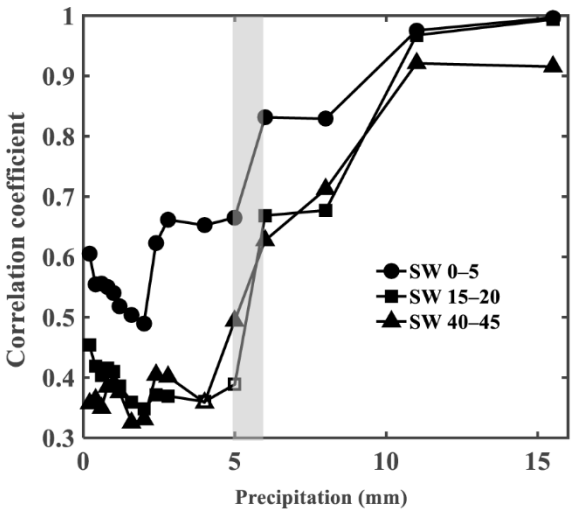

Figure 4. Correlation coefficients between $\delta^{18}O$ in soil water at depths of 0–5 (SW 0–5), 15–20 (SW 15–20), and 40–45 (SW 40–45) cm, and precipitation on the same day (n = 94). Open symbols indicate non-significant correlations, and solid ones indicate significant correlations at $p < 0.05$ level. Shadow areas indicate the critical thresholds of precipitation for infiltration into the soil profile.

3.3. Seasonal Variability in Residence Times of Precipitation in Soil

In spring, correlation coefficient between $\delta^{18}O$ in soil water at the 0–5 cm depth and $\delta^{18}O$ in cumulative precipitation ($R_{0–5}$) was highest at 0.89 at 0 days, indicating that $\delta^{18}O$ in soil water at the 0–5 cm depth was dominated by $\delta^{18}O$ in precipitation on that sampling day (Figure 5). Correlation coefficients between $\delta^{18}O$ in soil water at 15–20 ($R_{15–20}$) and 40–45 ($R_{40–45}$) cm depths and $\delta^{18}O$ in cumulative precipitation reached the highest values of 0.82 and 0.85 at 90 days, respectively. Highest $R_{0–5}$, $R_{15–20}$, and $R_{40–45}$ in winter were 0.78, 0.81, and 0.74 at 15, 60, and 60 days, respectively, and those in autumn were 0.79, 0.92, and 0.88 at 30, 60, and 105 days, respectively. Residence times of precipitation in soil in autumn were more than those in winter at depths of 0–5, 15–20, and 40–45 cm. Nevertheless, peak $R_{0–5}$, $R_{15–20}$, and $R_{40–45}$ at 0.67, 0.70, and 0.41 in 30, 60, and 105 days were low in summer as compared with those in other seasons, and it may be due to the combined influences of seasonal precipitation, soil evaporation, and plant transpiration. Residence times of precipitation in soil water increased with an increase in soil depth.

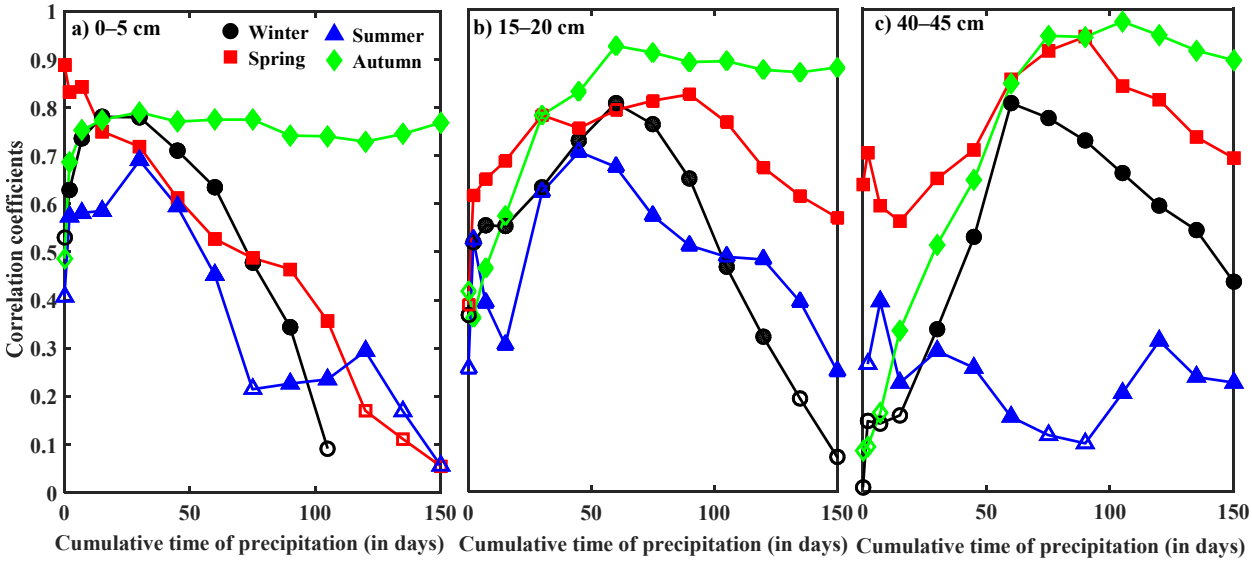

Figure 5. Correlation coefficients between $\delta^{18}O$ in soil water at depths of (**a**) 0–5 cm, (**b**) 15–20 cm, and (**c**) 40–45 cm, and $\delta^{18}O$ in cumulative precipitation (precipitation amount > 5 mm) before sampling during winter, spring, summer, and autumn. The x-axis represents the cumulative time of precipitation (in days), and x = 0 represents the correlation coefficient between $\delta^{18}O$ in soil water and precipitation in the same period. Open symbols indicate non-significant correlation, and solid symbols indicate significant correlation at $p < 0.05$.

3.4. Seasonal Variability of δ^2H and $\delta^{18}O$ in Soil Water Source

In winter, slopes of SEL calculated with the Craig and Gordon model-based approach at the 0–5 cm depth (CG 0–5) were significantly lower than those at depths of 15–20 (CG 15–20) and 40–45 (CG 40–45) cm (Figure 6). Slopes of CG 0–5, CG 15–20, and CG 40–45, which were 4.27, 5.27, and 5.65, respectively, were significantly lower than those calculated with the regression-based approach (7.05) in winter. Slopes of CG 0–5, CG 15–20, and CG 40–45, which were 4.13, 4.34, and 4.40, respectively, did not substantially differ, and were significantly lower than that calculated with the regression-based approach (7.00) in spring. Slopes of CG 0–5, CG 15–20, CG 40–45 and calculated with the regression-based approach in summer, which were 5.61, 5.94, 6.34, and 7.71, respectively, were similar to those in winter. In autumn, slopes of CG 0–5 (5.46) were significantly lower than those of CG 15–20 (5.90) and CG 40–45 (6.35) and calculated with the regression-based approach (6.47), and the latter three had no significant difference. A lower slope indicates a more enriched δ^2H and $\delta^{18}O$ in soil water source; δ^2H and $\delta^{18}O$ in the soil water source calculated with the two approaches for 0–5, 15–20, and 40–45 cm depths had opposite patterns (Table S3), except in autumn, when they were similar. Therefore, we conclude that both of the approaches can be used for calculating δ^2H and $\delta^{18}O$ in soil water source in autumn.

Based on the relationships between $\delta^{18}O$ in soil water source and precipitation (Figure 7 and Table S3), $\delta^{18}O$ in soil water source at the 0–5 cm depth in winter was close to the weighted average $\delta^{18}O$ in precipitation in autumn and winter, and $\delta^{18}O$ in soil water source in winter at 15–20 and 40–45 cm depths was close to the weighted average $\delta^{18}O$ in precipitation in summer and autumn. In spring, $\delta^{18}O$ in soil water source at 0–5 and 15–20 cm depths was close to the weighted average $\delta^{18}O$ in precipitation in winter and spring, while that at the 40–45 cm depth was similar to the weighted average $\delta^{18}O$ in precipitation in winter. All $\delta^{18}O$ in soil water source at 0–5, 15–20, and 40–45 cm depths in summer were close to the depleted weighted average $\delta^{18}O$ in precipitation in summer, while those at 0–5 and 15–20 cm depths were more depleted than those at the 40–45 cm depth. Nevertheless, $\delta^{18}O$ in soil water source at 0–5, 15–20, and 40–45 cm depths in autumn was close to the depleted weighted average $\delta^{18}O$ in precipitation in summer and autumn, and those at a depth of 0–5 cm were more enriched than those at 15–20 and 40–45 cm depths due to shorter residence times (more autumn precipitation recharge).

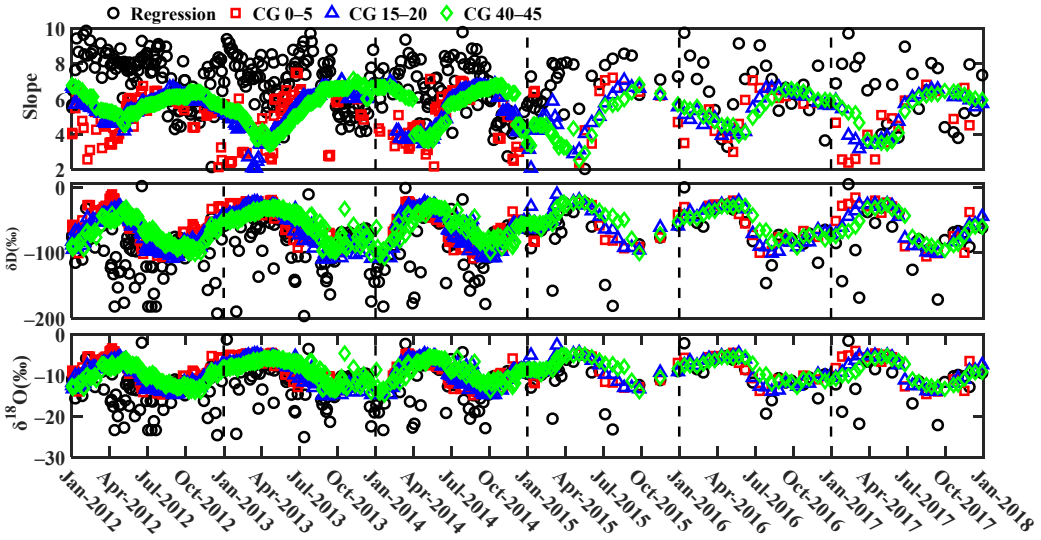

Figure 6. Temporal variability in the slopes of the soil water evaporation line, and δ^2H and $\delta^{18}O$ in soil water source calculated with the regression-based approach (open black circles; regression) and Craig and Gordon model-based approach at depths of 0–5 cm (open red squares; CG 0–5), 15–20 cm (open blue triangles; CG 15–20), and 40–45 cm (open green diamonds; CG 40–45).

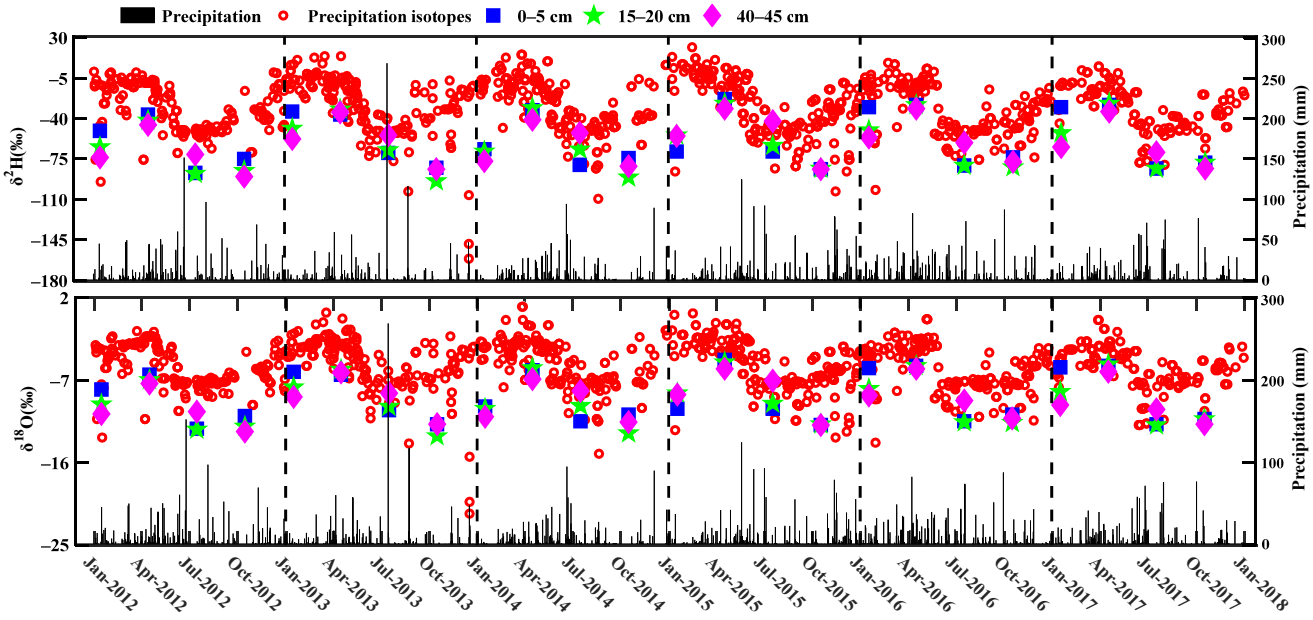

Figure 7. Temporal variability of the amount of precipitation, δ^2H and $\delta^{18}O$ in precipitation, and weighted average δ^2H and $\delta^{18}O$ in soil water source during winter, spring, summer, and autumn, at 0–5 (0–5 cm), 15–20 (15–20 cm), and 40–45 (40–45 cm) cm depths.

4. Discussion

4.1. Responses of Soil Water to Rainfall Events

Precipitation >5–6 mm passed through the canopy and litter layer, and infiltrated into soil in this subtropical plantation (Figure 4). This precipitation amount was slightly higher than that reported by Dai et al. [11], who showed that precipitation >3.7 mm led to a change in surface soil water content based on the regression equation of the variations in the soil water content from two consecutive days and daily precipitation. It may be due to more LAI (5.6 m^2/m^2) in this subtropical plantation than that (3.6 m^2/m^2) reported by Dai et al. [11]. However, Mello et al. [2] found that precipitation >1.58 mm could pass through the canopy layer (5.25 m^2/m^2) based on the linear regression of throughfall and

precipitation, without considering the litter layer. Existing studies have found that higher amounts of precipitation increased precipitation infiltration depths in grasses with a soil bulk density of 1.13–1.26 g/cm^3 [37], while the thresholds of precipitation for infiltration into soil at 0–5, 15–20, and 40–45 cm depths exhibited no significant differences in our study. However, the critical thresholds of precipitation for infiltration into the soil were closely related to vegetation and soil characteristics, and more LAI may cause a larger threshold.

Correlation coefficients between same-day $\delta^{18}O$ in soil water and precipitation increased with the increase in the amount of precipitation, and reached peak values when the amount of precipitation was 11 mm (Figure 4). This indicates that precipitation may mainly recharge soil-bound water before the formation of mobile water, or that hydrologic connectivity occurred, which was defined as the mixture between soil-bound water and soil mobile water [38], and the connectivity may increase with an increase in precipitation [39,40] when precipitation amount was less than a certain value. In addition, we found that peak correlation coefficients decreased with an increase in soil depths (Figure 4). One reason for this may be that before the formation of mobile water, precipitation infiltrating into the soil profile decreases due to an increase in initial soil water content with soil depths [41,42]. Another reason may be that there is little connectivity between soil-bound and mobile water due to ecohydrologic separation after the formation of mobile water, or some preferential flows when the amount of precipitation is larger than a certain value [40,43].

Nevertheless, it should be noted that the processes of evaporation, mixture with soil water having different signals of δ^2H and $\delta^{18}O$, and preferential flow may change the δ^2H and $\delta^{18}O$ of precipitation during the infiltration and influence the analysis of the precipitation threshold using the linkage between δ^2H and $\delta^{18}O$ in soil water and precipitation [8]. In addition, the incomplete extraction of soil water when soils contain a large percentage of silt and clay particles, or evaporation during the storage of soil samples, may cause certain uncertainties in the results [4].

4.2. Influencing Factors of Residence Times of Precipitation in Soil

In our study, residence times of precipitation in soil varied between a few days and several months, increased with the increase in soil depths, and were the shortest in spring and largest in autumn (Figure 5). It was possible that the connectivity of soil pores for precipitation infiltration, soil evaporation, and plant transpiration decreased with the increase in soil depth [15]. For a depth of 0–5 cm, the integrative effects of evapotranspiration and precipitation infiltration may result in a short residence time (<30 days). The seasonal variation of residence times at 15–20 and 40–45 cm depths may be caused by the pattern of seasonal precipitation in the East Asian monsoon region [11]. Precipitation inputs are the fundamental supply of "new water" in soil, and thus its variability can drive variations in the residence times of old water [44,45]. High precipitation amounts in spring in our study area resulted in short residence times in the soil in spring due to a large influx of "new water" and high soil water recharge, which could be retained until autumn. This was not the case in winter.

Nevertheless, the δ^2H and $\delta^{18}O$ in soil water was not only determined by the isotopic signals of precipitation inputs, but also by the mixture between the two and soil evaporation [46]. Therefore, the best correlation coefficients may not provide correct information about the residence time. In our study, R0–5, R15–20, and R40–45 in summer were low, and this may have been due to the influence of high soil evaporation. In addition to this correlation coefficient method, other approaches such as the simple classical sine curve or the new ensemble hydrograph separation approaches can also be used to determine the mean transit times [15].

4.3. Seasonal Origins of Soil Water

Slopes of SEL calculated with a regression-based approach were always higher than those calculated with the Craig and Gordon model-based approach in spring, summer,

and winter, while those slopes of SEL calculated with both approaches for autumn differed very little (Figure 6). An inverse variability in δ^2H and $\delta^{18}O$ in soil water source and soil evaporation fractionation may lead to higher slopes of SEL calculated with the regression-based approach than that calculated with the Craig and Gordon model-based approach [11,21,22,47]. In winter and spring, δ^2H and $\delta^{18}O$ in soil water source at the 0–5 cm depth were more enriched than those at depths of 15–20 and 40–45 cm due to recharge by enriched winter and spring precipitation, while the evaporation fractionation of soil water at 15–20 and 40–45 cm depths was higher than that at a depth of 0–5 cm due to the retention of autumn precipitation, which experienced high evaporation fractionation. In summer, the decrease in the depleted summer precipitation recharge of soil water led to a gradual enrichment of soil water source with soil depth, while the evaporation fractionation of δ^2H and $\delta^{18}O$ in soil water gradually decreased. Nevertheless, in autumn, both δ^2H and $\delta^{18}O$ in soil water source and evaporation fractionation at the 0–5 cm depth were more enriched than those at 15–20 and 40–45 cm depths. Above all, the occurrence of soil samples with depleted soil water source and high evaporation fractionation, and those with enriched soil water source and low evaporation fractionation along a soil profile may cause the overestimation of SEL slopes with the regression-based approach. Therefore, the SEL slopes calculated with the Craig and Gordon model-based approach were more robust than those calculated with the regression-based approach.

In winter, soil water at the 0–5 cm depth originated mainly from autumn and winter precipitation, while that at 15–20 and 40–45 cm depths originated primarily from summer and autumn precipitation (Figure 7). In spring, soil water at 0–5 and 15–20 cm depths originated mainly from winter and spring precipitation, while soil water at a depth of 40–45 cm only originated from winter precipitation. In summer, soil water in all layers was derived mainly from current precipitation. In autumn, soil water at the 0–5 cm depth originated mainly from autumn precipitation, while soil water at 15–20 and 40–45 cm depths originated mainly from summer and autumn precipitation. We conclude that soil water at the 0–5 cm depth originated primarily from precipitation in the current season, while soil water at 15–20 and 40–45 cm depths originated mainly from precipitation in the previous season in all seasons, except summer. Seasonal origins of soil water were similar to seasonal patterns of residence times. The widespread presence of summer and autumn precipitation in deep soils in winter indicates that these waters often resided in soils for several months [20,47].

5. Conclusions

The results of this study indicate that precipitation in this area need to be larger than 5–6 mm to pass through the canopy and litter layer, and then infiltrate into the soil. When precipitation amount was less than 11 mm, precipitation may mainly recharge soil-bound water before the formation of mobile water, or hydrologic connectivity between soil-bound and mobile water occurred, and connectivity increased with increasing precipitation. Residence times of precipitation in soil varied between a few days and several months, increased with soil depth, and were the shortest in spring and largest in autumn. These results may be due to the connectivity of soil pores for precipitation infiltration, soil evaporation, plant transpiration, and the seasonal pattern of precipitation in the East Asian monsoon region. Slopes of SEL calculated with the Craig and Gordon model-based approach were more robust than those calculated with the regression-based approach due to the inverse variation in δ^2H and $\delta^{18}O$ in soil water source and soil evaporation fractionation. Nevertheless, the SEL slopes calculated with the two approaches differed little in autumn. δ^2H and $\delta^{18}O$ in soil water source and precipitation indicated that soil water at the 0–5 cm depth originated mainly from precipitation in the current season, while soil water in all seasons except summer at depths of 15–20 and 40–45 cm originated mainly from precipitation in the previous season. Our results highlight that precipitation in the previous season is important for alleviating the decreasing water availability during the autumn and winter seasons in the East Asian monsoon region.

Supplementary Materials: The following are available online at https://www.mdpi.com/article/10.3390/w13202930/s1, Table S1: The slopes (a) and intercepts (b), together with standard deviations (SD) of local meteoric water lines (LMWL), the average Root Mean Sum of Squared Error ($RMSE_{av}$) value of the fit, the number of samples (n) and the significance in the difference of each regression to that of OLSR (*p*-value), when the ordinary least squares regression (OLSR), reduced major axis regression (RMA), major axis regression (MA), and the corresponding precipitation weighted regressions (PWLSR, PWRMA and PWMA) were used, in spring, summer, autumn and winter, Table S2: The δ^2H and $\delta^{18}O$ in soil water at 0–5 (SW 0–5), 15–20 (SW 15–20), and 40–45 (SW 40–45) cm depths, and precipitation of different rainfall intensity during winter, spring, summer and autumn, Table S3: The δ^2H and $\delta^{18}O$ of soil water source by regression-based approach (Source Obs) and Craig and Gordon model-based approach at 0–5 (Source CG 0–5), 15–20 (Source CG 15–20), and 40–45 (Source CG 40–45) cm depths, and δ^2H and $\delta^{18}O$ in precipitation (precipitation amount>5 mm), during winter, spring, summer and autumn.

Funding: This research was funded by the National Natural Science Foundation of China, grant number 41807167 and 41830860.

Institutional Review Board Statement: Not applicable.

Informed Consent Statement: Not applicable.

Data Availability Statement: The data of δ^2H and $\delta^{18}O$ in soil water and precipitation presented in this study are available on request from the corresponding author. Auxiliary meteorological data in this study can be found in the publicly available datasets: [http://qya.cern.ac.cn/ accessed on 18 September 2021].

Acknowledgments: The author thanks Qianyanzhou Ecological Experimental Station for laboratory assistance and for the collection of soil and precipitation samples.

Conflicts of Interest: The author declares no conflict of interest.

References

1. Brooks, J.R. Water, bound and mobile. *Science* **2015**, *349*, 138–139. [CrossRef] [PubMed]
2. Mello, C.R.; Avila, L.F.; Lin, H.; Terra, M.C.N.S.; Chappell, N.A. Water balance in a neotropical forest catchment of southeastern Brazil. *Catena* **2019**, *173*, 9–21. [CrossRef]
3. McColl, K.A.; Alemohammad, S.H.; Akbar, R.; Konings, A.G.; Yueh, S.; Entekhabi, D. The global distribution and dynamics of surface soil moisture. *Nat. Geosci.* **2017**, *10*, 100–104. [CrossRef]
4. Sprenger, M.; Leistert, H.; Gimbel, K.; Weiler, M. Illuminating hydrological processes at the soil-vegetation-atmosphere interface with water stable isotopes. *Rev. Geophys.* **2016**, *54*, 674–704. [CrossRef]
5. Ellsworth, P.Z.; Williams, D.G. Hydrogen isotope fractionation during water uptake by woody xerophytes. *Plant Soil* **2007**, *291*, 93–107. [CrossRef]
6. Lyu, S.; Wang, J.; Song, X.; Wen, X. The relationship of δD and $\delta^{18}O$ in surface soil water and its implications for soil evaporation along grass transects of Tibet, Loess, and Inner Mongolia Plateau. *J. Hydrol.* **2021**, *600*, 126533. [CrossRef]
7. Craig, H. Isotopic variations in meteoric waters. *Science* **1961**, *133*, 1702–1703. [CrossRef]
8. Sprenger, M.; Tetzlaff, D.; Buttle, J.; Carey, S.K.; McNamara, J.P.; Laudon, H.; Shatilla, N.J.; Soulsby, C. Storage, mixing, and fluxes of water in the critical zone across northern environments inferred by stable isotopes of soil water. *Hydrol. Process.* **2018**, *32*, 1720–1737. [CrossRef]
9. Liu, X.; He, Y.; Zhang, T.; Zhao, X.; Li, Y.; Zhang, L.; Wei, S.; Yun, J.; Yue, X. The response of infiltration depth, evaporation, and soil water replenishment to rainfall in mobile dunes in the Horqin Sandy Land, Northern China. *Environ. Earth Sci.* **2015**, *73*, 8699–8708. [CrossRef]
10. Cuartas, L.A.; Tomasella, J.; Nobre, A.D.; Hodnett, M.G.; Waterloo, M.J.; Munera, J.C. Interception water-partitioning dynamics for a pristine rainforest in Central Amazonia: Marked differences between normal and dry years. *Agric. For. Meteorol.* **2007**, *145*, 69–83. [CrossRef]
11. Dai, J.J.; Zhang, X.P.; Luo, Z.D.; Wang, R.; Liu, Z.L.; He, X.G.; Rao, Z.G.; Guan, H.D. Variation of the stable isotopes of water in the soil-plant-atmosphere continuum of a Cinnamomum camphora woodland in the East Asian monsoon region. *J. Hydrol.* **2020**, *589*, 125199. [CrossRef]
12. Brooks, J.R.; Barnard, H.R.; Coulombe, R.; McDonnell, J.J. Ecohydrologic separation of water between trees and streams in a Mediterranean climate. *Nat. Geosci.* **2010**, *3*, 100–104. [CrossRef]
13. Hervé-Fernández, P.; Oyarzún, C.; Brumbt, C.; Huygens, D.; Bodé, S.; Verhoest, N.E.C.; Boeckx, P. Assessing the "two water worlds" hypothesis and water sources for native and exotic evergreen species in south-central Chile. *Hydrol. Process.* **2016**, *30*, 4227–4241. [CrossRef]

14. Maxwell, R.M.; Condon, L.E. Connections between groundwater flow and transpiration partitioning. *Science* **2016**, *353*, 377–380. [CrossRef] [PubMed]
15. Sprenger, M.; Stumpp, C.; Weiler, M.; Aeschbach, W.; Allen, S.T.; Benettin, P.; Dubbert, M.; Hartmann, A.; Hrachowitz, M.; Kirchner, J.W.; et al. The demographics of water: A review of water ages in the critical zone. *Rev. Geophys.* **2019**, *57*, 800–834. [CrossRef]
16. Brinkmann, N.; Seeger, S.; Weiler, M.; Buchmann, N.; Eugster, W.; Kahmen, A. Employing stable isotopes to determine the residence times of soil water and the temporal origin of water taken up by Fagus sylvatica and Picea abies in a temperate forest. *New Phytol.* **2018**, *219*, 1300–1313. [CrossRef]
17. Allen, S.T.; Kirchner, J.W.; Braun, S.; Siegwolf, R.T.W.; Goldsmith, G.R. Seasonal origins of soil water used by trees. *Hydrol. Earth Syst. Sci.* **2019**, *23*, 1199–1210. [CrossRef]
18. Dudley, B.D.; Marttila, H.; Graham, S.L.; Evison, R.; Srinivasan, M.S. Water sources for woody shrubs on hillslopes: An investigation using isotopic and sapflow methods. *Ecohydrology* **2018**, *11*, e1926. [CrossRef]
19. Evaristo, J.; Jasechko, S.; McDonnell, J.J. Global separation of plant transpiration from groundwater and streamflow. *Nature* **2015**, *525*, 91–94. [CrossRef]
20. Benettin, P.; Volkmann, T.H.M.; von Freyberg, J.; Frentress, J.; Penna, D.; Dawson, T.E.; Kirchner, J. Effects of climatic seasonality on the isotopic composition of evaporating soil waters. *Hydrol. Earth Syst. Sc.* **2018**, *22*, 2881–2890. [CrossRef]
21. Xiang, W.; Evaristo, J.; Li, Z. Recharge mechanisms of deep soil water revealed by water isotopes in deep loess deposits. *Geoderma* **2020**, *369*, 114321. [CrossRef]
22. Yu, G.; Chen, Z.; Piao, S.; Peng, C.; Ciais, P.; Wang, Q.; Li, X.; Zhu, X. High carbon dioxide uptake by subtropical forest ecosystems in the East Asian monsoon region. *Proc. Natl. Acad. Sci. USA* **2014**, *111*, 4910–4915. [CrossRef] [PubMed]
23. Song, X.; Lyu, S.; Wen, X. Limitation of soil moisture on the response of transpiration to vapor pressure deficit in a subtropical coniferous plantation subjected to seasonal drought. *J. Hydrol.* **2020**, *591*, 125301. [CrossRef]
24. Tang, Y.K.; Wen, X.F.; Sun, X.M.; Zhang, X.Y.; Wang, H.M. The limiting effect of deep soil water on evapotranspiration of a subtropical coniferous plantation subjected to seasonal drought. *Adv. Atmos. Sci.* **2014**, *31*, 385–395. [CrossRef]
25. Yang, B.; Wen, X.; Sun, X. Seasonal variations in depth of water uptake for a subtropical coniferous plantation subjected to drought in an East Asian monsoon region. *Agric. For. Meteorol.* **2015**, *201*, 218–228. [CrossRef]
26. Yang, F.; Feng, Z.; Wang, H.; Dai, X.; Fu, X. Deep soil water extraction helps to drought avoidance but shallow soil water uptake during dry season controls the inter-annual variation in tree growth in four subtropical plantations. *Agric. For. Meteorol.* **2017**, *234*, 106–114. [CrossRef]
27. Wen, X.F.; Yu, G.R.; Sun, X.M.; Li, Q.K.; Liu, Y.F.; Zhang, L.M.; Ren, C.Y.; Fu, Y.L.; Li, Z.Q. Soil moisture effect on the temperature dependence of ecosystem respiration in a subtropical Pinus plantation of southeastern China. *Agric. For. Meteorol.* **2006**, *137*, 166–175. [CrossRef]
28. West, A.G.; Patrickson, S.J.; Ehleringer, J.R. Water extraction times for plant and soil materials used in stable isotope analysis. *Rapid Commun. Mass Spectrom.* **2006**, *20*, 1317–1321. [CrossRef]
29. Wen, X.; Lee, X.; Sun, X.; Wang, J.; Tang, Y.; Li, S.; Yu, G. Intercomparison of four commercial analyzers for water vapor isotope measurement. *J. Atmos. Ocean. Technol.* **2012**, *29*, 235–247. [CrossRef]
30. Nelson, D.B.; Basler, D.; Kahmen, A. Precipitation isotope time series predictions from machine learning applied in Europe. *Proc. Natl. Acad. Sci. USA* **2021**, *118*, e2024107118. [CrossRef]
31. Allison, G.B. The relationship between O-18 and deuterium in water in sand columns undergoing evaporation. *J. Hydrol.* **1982**, *55*, 163–169. [CrossRef]
32. Gibson, J.J.; Birks, S.J.; Edwards, T.W.D. Global prediction of δA and δ^2H-δ^{18}O evaporation slopes for lakes and soil water accounting for seasonality. *Global Biogeochem. Cycles* **2008**, *22*, GB2031. [CrossRef]
33. Horita, J.; Wesolowski, D.J. Liquid-vapor fractionation of oxygen and hydrogen isotopes of water from the freezing to the critical-temperature. *Geochim. Cosmochim. Acta* **1994**, *58*, 3425–3437. [CrossRef]
34. Gat, J.R. Oxygen and hydrogen isotopes in the hydrologic cycle. *Annu. Rev. Earth Planet. Sci.* **1996**, *24*, 225–262. [CrossRef]
35. Crawford, J.; Hughes, C.E.; Lykoudis, S. Alternative least squares methods for determining the meteoric water line, demonstrated using GNIP data. *J. Hydrol.* **2014**, *519*, 2331–2340. [CrossRef]
36. He, Z.M.; Jia, G.D.; Liu, Z.Q.; Zhang, Z.Y.; Yu, X.X.; Hao, P.Q. Field studies on the influence of rainfall intensity, vegetation cover and slope length on soil moisture infiltration on typical watersheds of the Loess Plateau, China. *Hydrol. Process.* **2020**, *34*, 4904–4919. [CrossRef]
37. Luo, Z.D.; Guan, H.D.; Zhang, X.P.; Xu, X.; Dai, J.J.; Hua, M.Q. Examination of the ecohydrological separation hypothesis in a humid subtropical area: Comparison of three methods. *J. Hydrol.* **2019**, *571*, 642–650. [CrossRef]
38. Good, S.P.; Noone, D.; Bowen, G. Hydrologic connectivity constrains partitioning of global terrestrial water fluxes. *Science* **2015**, *349*, 175–177. [CrossRef]
39. Radolinski, J.; Pangle, L.; Klaus, J.; Stewart, R.D. Testing the 'two water worlds' hypothesis under variable preferential flow conditions. *Hydrol. Process.* **2021**, *35*, e14252. [CrossRef]
40. Knighton, J.; Souter-Kline, V.; Volkman, T.; Troch, P.A.; Kim, M.; Harman, C.; Morris, C.; Buchanan, B.; Walter, M.T. Seasonal and topographic variations in ecohydrological separation within a small, temperate, snow-influenced catchmet. *Water Resour. Res.* **2019**, *55*, 6417–6435. [CrossRef]

41. Lyu, S.D.; Song, X.W.; Wen, X.F. Ecohydrologic separation of the mixing process between precipitation and soil water: A review. *Chin. J. Appl. Ecol.* **2019**, *30*, 1797–1806.
42. Qian, J.; Zheng, H.; Wang, P.F.; Liao, X.L.; Wang, C.; Hou, J.; Ao, Y.H.; Shen, M.M.; Liu, J.J.; Li, K. Assessing the ecohydrological separation hypothesis and seasonal variations in water use by Ginkgo biloba L. in a subtropical riparian area. *J. Hydrol.* **2017**, *553*, 486–500. [CrossRef]
43. Wilusz, D.C.; Harman, C.J.; Ball, W.P. Sensitivity of catchment transit times to rainfall variability under present and future climates. *Water Resour. Res.* **2017**, *53*, 10231–10256. [CrossRef]
44. Evaristo, J.; Kim, M.; van Haren, J.; Pangle, L.A.; Harman, C.J.; Troch, P.A.; McDonnell, J.J. Characterizing the fluxes and age distribution of soil water, plant water and deep percolation in a model tropical ecosystem. *Water Resour. Res.* **2019**, *55*, 3307–3327. [CrossRef]
45. Stockinger, M.P.; Luecke, A.; McDonnell, J.J.; Diekkrueger, B.; Vereecken, H.; Bogena, H.R. Interception effects on stable isotope driven streamwater transit time estimates. *Geophys. Res. Lett.* **2015**, *42*, 5299–5308. [CrossRef]
46. Tetzlaff, D.; Buttle, J.; Carey, S.K.; Kohn, M.J.; Laudon, H.; McNamara, J.P.; Smith, A.; Sprenger, M.; Soulsby, C. Stable isotopes of water reveal differences in plant—Soil water relationships across northern environments. *Hydrol. Process.* **2021**, *35*, e14023. [CrossRef]
47. Jin, Z.; Guo, L.; Lin, H.; Wang, Y.; Yu, Y.; Chu, G.; Zhang, J. Soil moisture response to rainfall on the Chinese Loess Plateau after a long-term vegetation rehabilitation. *Hydrol. Process.* **2018**, *32*, 1738–1754. [CrossRef]